



Kinetic and isotherm studies for adsorption of Pb(II) from aqueous solution onto coconut shell activated carbon

G.E. Sharaf El-Deen^a, S.E.A. Sharaf El-Deen^{b,*}

^aHot Laboratories Center, Department of Radioactive Waste Management, Atomic Energy Authority, P.O. Box 13759, Inshas, Egypt

^bHot Laboratories Center, Department of Nuclear Chemistry, Atomic Energy Authority, P.O. Box 13759, Inshas, Egypt,
Tel. +2 010 09846926; Fax: +2 4620806; email: sahar97@gmail.com (S.E.A. Sharaf El-Deen)

Received 5 December 2015; Accepted 19 May 2016

ABSTRACT

Coconut shell (CS) was used as a neglected agricultural waste to produce the activated carbon through chemical activation process with phosphoric acid (activated coconut shell (ACS)). This process is easy and environmental friendly. The activated carbon (ACS) as biosorbent was evaluated for sorption of lead from wastewater using a series of batch adsorption experiments and compared with pyrolysis CS. The characterization results showed that this biosorbent (ACS) has high surface area and functional groups. The efficiency of adsorption process was studied at various parameters: pH, contact time, initial concentration, and competing ions for the removal of Pb(II) ions from aqueous solution. Adsorption equilibrium data were analyzed by the two parameters models (Langmuir, Freundlich, Temkin, and R–D) and the three parameters models (Generalized, Toth, Radke–Prausnitz, and Fritz–Schlunder models). The adsorption equilibrium data was well described by Langmuir and the monolayer adsorption capacities were found to be 49.92 and 26.14 mg/g onto ACS and CS, respectively, which are agreement with those obtained from the three-parameter isotherm models. The experimental kinetic data were best fitted with Bangham's, Weber–Morris and pseudo-second-order models. The diffusion mechanism was controlled by both boundary layer and pore diffusion for the two adsorbents CS and ACS. It is noteworthy that the effect of Cd(II) and Fe(III) on the adsorption of Pb(II) is very weak, even with high concentration of Cd(II) or Fe(III), which means that the investigated adsorbents have higher affinity for sorption of Pb(II) than that of the other competing ions. The results showed that ACS can be used as a low-cost adsorbent for the removal of Pb(II) ions from aqueous solutions.

Keywords: Coconut shell; Activated carbon; Adsorption isotherm; Kinetics; Lead removal

1. Introduction

The removal of toxic metal ions from wastewater is an important and widely studied research area. Lead is considered as one of the dangerous toxic

metal ions, due to its severe toxicity and great potential hazard to the environment and organisms [1]. Lead is used on a large scale in building materials, storage batteries, bullets, mining, plating, lead smelting and ceramic glass industries, and it can damage the nervous systems and reproductive health for the human [2]. According to USEPA, the permissible level

*Corresponding author.

of Pb(II) in drinking water is 0.015 mg/L [3]. The increasing of lead concentration in drinking water than the permissible level causes some diseases such as anemia, encephalopathy, and inflammation of the kidney and liver. Therefore, the removal and elimination of lead from contaminated water and wastewater is necessary for protection of the environment and human health.

Various treatment methods have been used to remove lead from wastewater such as chemical precipitation, solvent extraction, reverse osmosis, ion exchange, filtration, adsorption, and membrane processes [4–11]. While most of previously described treatment methods have some disadvantages like high operational cost, low treatment efficiency, and production of secondary waste products that also need treatment process [7]. Adsorption is a promising process due to its high effective, easy operation, fast and economical method for removal of Pb(II) from aqueous solutions.

Activated carbons are often used as porous adsorbents for treatment of aqueous wastes contaminated with toxic metal ions because of their higher surface area, high adsorption capacity, microporous structure, and active functional groups such as carboxylic, hydroxyl, carbonyl, phenolic, aldehyde, and other organic functional groups that existed on the edges of hexagonal carbon layer planes [12,13]. In aqueous solutions, these functional groups can be ionized depending on the pH-value, leading to the creation of charge interface between the adsorbent surface and the bulk of solution [12].

In recent years, the main focus is on the use of various industrial wastes and agricultural byproducts as adsorbent for the removal of Pb(II) from wastewater. Natural materials that are available in large quantities or certain waste from agricultural operation is getting increased attention all over the world as they are cheap, widely available, renewable, unused resources, and environmental friendly. Agricultural byproducts like pine cone [12], apricot stone [14], sawdust [15], bamboo charcoal [16], rubber leaf powder [17], sugarcane bagasse [18–20], African palm pit [18], coconut shell (CS) [21–24], and bagasse coconut [25] have been successfully used for preparation of activated carbons.

From 1980 to the 2010, the total coconut production in the world wide increased greatly from 35 to 50 million tons [21]. Adsorption onto CS activated carbon as low-cost adsorbent gives great and inexpensive choice for the removal of lead. The abundance and availability of CS makes it economically feasible.

This paper studies the adsorption of Pb(II) from aqueous solutions onto activated carbon prepared from coconut shell (activated coconut shell (ACS)) and compare with the pyrolysis CS. Kinetic and equilibrium studies are discussed.

2. Materials and methods

2.1. Adsorbent preparation

CSs were obtained locally from Delta Company for sweets and industrial foods “Jammy”, Tenth of Ramadan City, Sharqia governorate, Egypt and used as a precursor for preparation of two adsorbents using pyrolysis and chemical activation methods as shown in Fig. 1. Firstly, the shells were crushed into small pieces, washed with double distilled water, and dried in oven at 110°C for 6 h. then sieved to desired mesh size of 1 mm. Secondly, fifty gram of CS were placed in stainless steel tube reactor and heated up to 600°C gradually at rate of 50°C/15 min, and hold time for 2 h. After reaching the final pyrolysis temperature, the reactor was set to cool to room temperature. The pyrolysis CS was obtained and taken the abbreviation (CS). Another fifty gram of CS was impregnated with certain amount of 80 vol.% H₃PO₄ for 24 h. The impregnated solid was filtered, then transferred to a stainless steel tube reactor and heated up to 500°C gradually with heating rate of 50°C/15 min and the sample was held at the carbonization temperature for 2 h. Then the furnace was switched off and the sample was left to cool down. The cold activated product was washed with distilled water to remove all the free acid until a neutral pH was obtained and then dried at 110°C for 24 h. The final product was weighed and designated as coconut shell activated carbon (ACS).

2.2. Characterization of adsorbents

The adsorbents, coconut shell activated carbon (ACS) and pyrolysis CS were characterized with Fourier transform infra-red spectroscopy (FTIR) (Perkin Elmer Spectrum 100). The porous texture of samples was determined by liquid N₂ adsorption at 77 K using the surface area analyzer (Nova 1000e series, USA). Texture parameters were determined by applying the BET-equation (S_{BET}), total pore volume (V_p) held at $P/P_0 = 0.95$, and average pore radius from the relationship $r = 2V_p/S_{\text{BET}}$. The morphology properties of the samples were examined by JEOL analytical scanning electron microscope (SEM, JSM-6510 LA, Japan) equipped with an EDX detector.

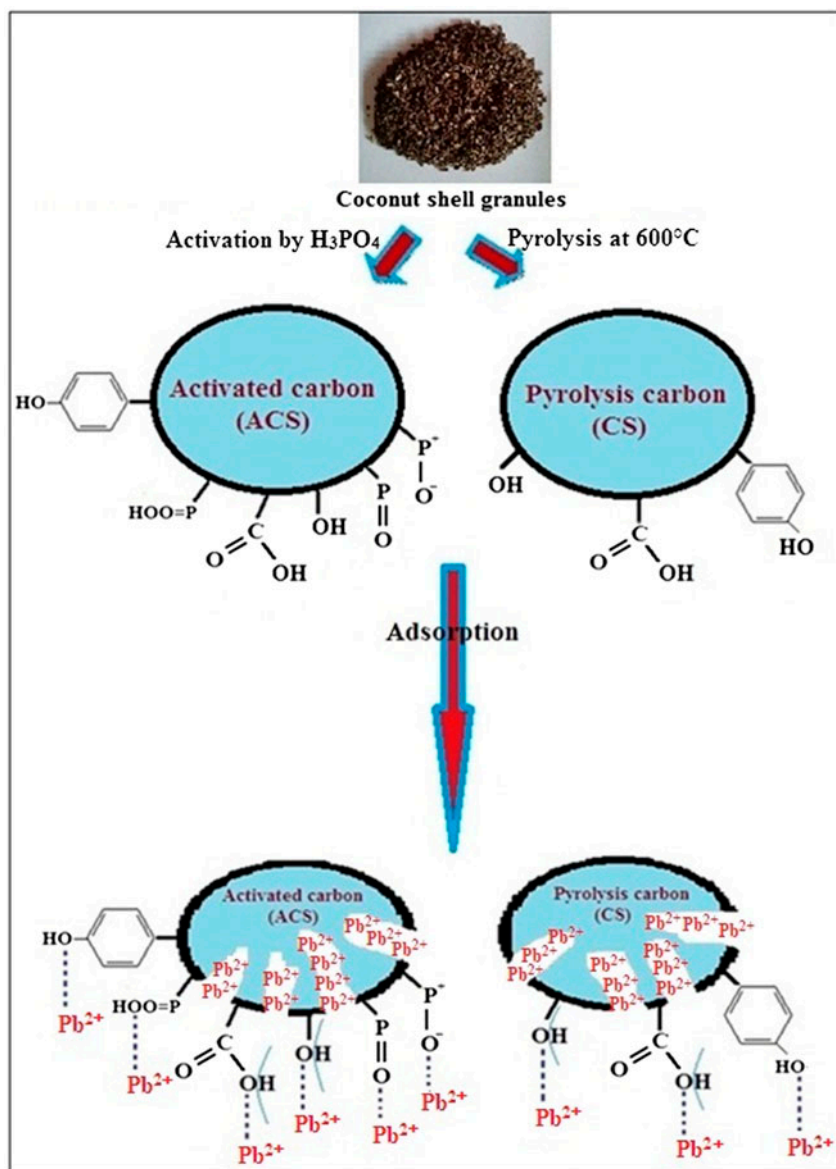


Fig. 1. Schematic representation of preparation of activated coconut shell ACS and pyrolysis CS and their Pb(II) adsorption mechanism.

2.3. Determination method of zero-point charge (pH_{ZPC}) of the adsorbents

To define the pH_{ZPC}, certain amount (0.1 g) of the adsorbent (CS or ACS) was added to 50 ml of 0.2 mol/L NaCl solution, used as an inert electrolyte in 100 ml stoppered conical flask. The initial pH of solution was adjusted to pH from 2 to 10 using 0.1 mol/L NaOH or 0.1 mol/L HCl solution. Then the mixture was shaking for 24 h at 250 r/min. in shaker at room temperature (21 ± 1)°C. After equilibrium, the mixture was filtered and the zeta potential was measured using a Zetamaster potentiometer (Malvern Instruments, UK).

2.4. Batch adsorption experiment

A stock solution of 1,000 mg/L Pb(II) was prepared from a known quantity of analytical-grade lead nitrate (Pb(NO₃)₂) dissolved in deionized water. The pH values were adjusted with 0.1 M HCl or 0.1 M NaOH solution, and all of the pH measurements were carried out using a pH meter (DELTA 320, METTLER). The adsorption of Pb(II) onto ACS and CS was studied by the batch technique. A thermostatic shaker (THZ-100, Shanghai Yiheng Scientific Instrument Company) was used for adsorption experiments.

In the adsorption equilibrium, experiments were conducted by adding a fixed amount of carbons (ACS and CS) (0.02 g) into 50 ml Erlenmeyer flasks containing 20 ml of different initial concentrations (5–50 mg/L) of Pb(II) solution. The flasks were agitated in a thermostatic shaker at 200 rpm, at 25°C for 24 h. to reach equilibrium of the solid-solution mixture. The samples were then filtrated and measured using atomic absorption spectroscopy (AAS) (Perkin Elmer, Analyzer 300). The adsorption capacity of Pb(II), q_e (mg/g), and the adsorption percentage were calculated as follows (Eqs. (1) and (2)):

$$q_e = \frac{(C_0 - C_e)V}{m} \quad (1)$$

$$\text{Adsorption \%} = \frac{C_0 - C_e}{C_0} \times 100 \quad (2)$$

where C_0 and C_e are the initial and equilibrium concentrations (mg/g), V is the volume of solution (L), m is the mass of the carbon material (g).

In order to evaluate the effect of pH on Pb(II)-ions adsorption, the initial pH values of a series from 20 ml of 20 ppm Pb(II) solutions were varied between 2 and 7 by adjusting with 0.1 M HCl and 0.1 M NaOH at 25°C and added into different flasks. 0.02 g of the adsorbent was then added to each flask, and then agitated at a speed of 250 rpm for 24 h. The optimum pH was then determined and used throughout all the adsorption experiments.

Several adsorption isotherm models were investigated such as: Langmuir, Freundlich, Temkin, and Dubinin–Kaganer–Radushkevich (D–R) isotherms in linear and nonlinear form and Generalized, Toth, Radke–Prausnitz and Fritz–Schlunder isotherms in nonlinear form. To investigate the adsorption isotherm, 0.02 g of both of ACS and CS was added to each flask containing on 20 ml of Pb(II) solutions with different concentrations 5–50 mg/L at pH 5.5. The conical flasks mounted on a shaker at 250 rpm for a specified time. Then, the aqueous samples were filtered and the Pb (II) concentrations were measured using AAS.

In this work, different adsorption kinetic models, such as pseudo-first-order, pseudo-second-order, Elovich, and mass transfer diffusion models (Mathews–Weber, Bangham's, Vermeulen's, and Weber–Morris's diffusion models) were studied. To study the adsorption kinetic of Pb(II)- ions, 0.02 g of each ACS and CS was added to 20 ml of 20 mg/L Pb(II) aqueous solution at pH 5. The experiment was carried out in a manner similar to that described above. Each experiment was carried out in triplicate and the average results are presented in this work.

3. Results and discussion

3.1. Characterization of CS and ACS

3.1.1. Fourier transforms infrared (FTIR) spectroscopy

The FTIR spectrum of CS and ACS is illustrated in Fig. 2. A wide absorption band at 3,200–3,600 cm^{-1} with a maximum at about 3,432 and 3,419 cm^{-1} are assigned to O–H stretching vibrations of hydroxyl groups and adsorbed water. Aliphatic C–H stretching vibration is found as a very weak peak at 2,847 cm^{-1} while asymmetric vibration of CH_2 group appears at 2,922 cm^{-1} . A peak around 1,620 cm^{-1} can be ascribed to C=O stretching vibrations of ketones, aldehydes, lactones, or carboxyl groups.

For ACS, the broadbands at 1,300–1,000 cm^{-1} may originate from phosphoric compounds developed due to H_3PO_4 activation. According to this, the peak at 1,175 cm^{-1} is attributed to the stretching vibrations of hydrogen bonded P=O, stretching vibrations of O–C in P–O–C linkage, and P=OOH. The small shoulder around 1,033 cm^{-1} is attributed to ionized linkage $\text{P}^+ \text{--} \text{O}^-$ in acid phosphate and to symmetrical vibration in a chain of P–O–P [12]. Bands that appear below 900 cm^{-1} are characteristics of aromatic structures or P–C phosphorus-containing compound [7]. The activation using H_3PO_4 , leads to increase the oxygen-containing functional groups including acidic hydroxyl, carboxyl, phenolic hydroxyl, and phosphate groups on the carbon surface.

3.1.2. Pore structure characterization

3.1.2.1. Nitrogen adsorption–desorption isotherms. The nitrogen adsorption–desorption isotherm at 77 K is

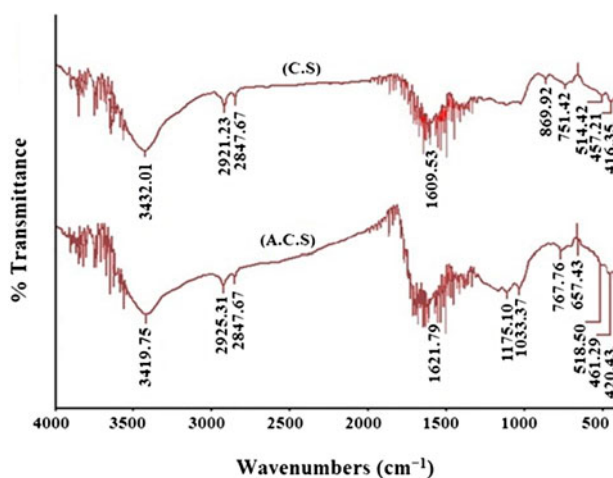


Fig. 2. FTIR of pyrolysis CS and ACS.

illustrated in Fig. 3 as a relation between the relative pressure (P/P_0) and the volume (V) for the two adsorbents (CS and ACS) to estimate several porosity parameters, which are compiled in Table 1. Fig. 3 shows that all isotherms are belonging to type IV according to IUPAC classification with a hysteresis loop typical of mesoporous materials [26]. The shape of the low-pressure portion of the isotherms depends on the microporosity of carbon surface [27]. A more rounded knee appearing in most of the isotherms indicate a widening of the microporosity that extend to high degree of mesoporosity which conformed by appearing of hysteresis loop in their isotherms [28].

3.1.2.2. Pore size distribution. Fig. 4 indicates that the samples exhibit wide pore size distribution, from narrow micropores to wide mesopores. The peak in the region of 1 nm indicates the micropore region where one model distribution of pore size is obtained in the two samples. For mesopore region, a broad pore size distribution was observed with two minima at about

2.2 and 3.6 nm corresponding to the transition from pore wide accommodating one adsorbed layer to two, and two layer to three, respectively [28].

From Table 1, the activated carbon (ACS) has higher micropores structure than of CS. This is due to the low surface area of CS ($S_{\text{BET}} = 19 \text{ m}^2/\text{g}$) than the surface area of activated carbon (ACS) ($S_{\text{BET}} = 624 \text{ m}^2/\text{g}$).

The data indicate that the resulting carbon (ACS) showed reasonable surface area with mainly micropore structure. Thus, the production of activated carbon from agricultural by-products serves a double purpose. Firstly, it converts unwanted, surplus agricultural waste, of which billions of kilograms are produced annually, to useful, value-added adsorbents. Secondly, the activated carbon can be used in aqueous phase applications e.g. wastewater treatment plants. Consequently, production of activated carbon derived from CS had been demonstrated to be feasible. However, activation by H_3PO_4 followed by pyrolysis at 500°C proved very effective in producing a good quality activated carbon with well-developed porosity.

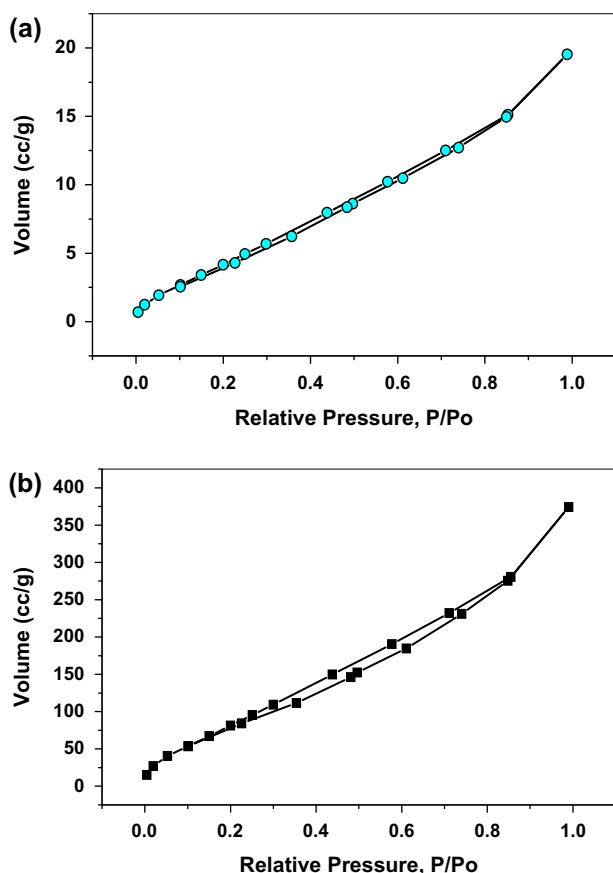


Fig. 3. Nitrogen adsorption–desorption isotherms at 77 K for (a) CS and (b) ACS.

3.1.2.3. SEM and EDX-characterization. The SEM/EDX images of ACS with and without adsorbed Pb(II) ions are shown in Fig. 5. SEM photo of ACS without adsorbed Pb(II) shows irregular granules of activated carbon with each other as conglomerates of ACS granules, Fig. 5(a). While for samples of ACS adsorbed Pb(II) ions, the SEM examination detected that the inorganic portions of the adsorbed Pb(II) ions consist of dark gray regular balls, Fig. 5(c). Also the image shows the pores as channels inside the granules of ACS sample. However, EDX results show interesting differences in the two samples (prepared ACS before and after Pb^{2+} adsorption) as shown in Fig. 5(b) and (d). EDX spectroscopy confirms that there is a good amount of lead ions in ACS/Pb(II) samples after adsorption of Pb(II) ions.

3.1.3. Determination of pH_{ZPC} of the two adsorbents (CS and ACS)

The pH_{ZPC} is a concept relating to the phenomenon of adsorption. pH_{ZPC} can be defined as the pH value at which a solid submerged in an electrolyte exhibits zero net electrical charge on the surface. As noticed in Fig. 6, the pH_{ZPC} values are approximately 4.2 and 3.3 for CS and ACS, respectively. This announced that the activation by phosphoric acid increases the acidic properties of ACS according to hydrogen bonded $\text{P}=\text{O}$, $\text{P}=\text{OOH}$ and $\text{P}-\text{O}-\text{P}$ functional groups.

Table 1
Several porous characteristics of the adsorbents

Adsorbent	Micropores (%)	Mesopores (%)	S_{BET} (m^2/g)	V_p (mL/g)	Average pore radius (r , \AA)
CS	52.9	47.1	19.0114	0.01	10.52
ACS	79.2	20.8	624	0.4492	14.39

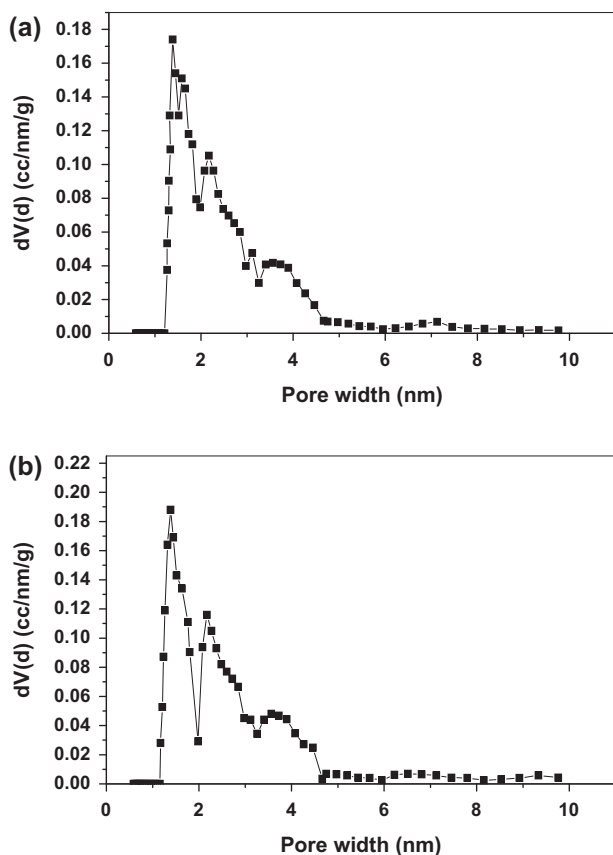


Fig. 4. DFT pore size distribution of (a) pyrolysis CS and (b) ACS.

3.2. Adsorption studies of Pb(II) onto CS and ACS

3.2.1. Contact time

The influence of contact time on the adsorption of Pb(II) on both of CS and ACS was studied and the results are represented in Fig. 7. The adsorption of Pb(II) onto CS and ACS increases with time and then attains equilibrium value at a time of about 3 h. The maximum adsorption reached to 94.7 and 56.55% at equilibrium for ACS and CS, respectively. Further increase in contact time did not show an increase in adsorption. Thus, 3 h. shaking time was considered to be the optimum contact time for adsorption of Pb(II) on the adsorbents.

3.2.2. pH dependence

It is known that the pH of a solution is considered as a very important controlling parameter in the adsorption process. Where, it affects the degree of ionization of the surface functional groups which define the surface charge and also influences on the speciation of metal ions. The batch experimental method was used to determine the effect of pH on adsorption of Pb(II) on the two adsorbents, at initial Pb(II) concentration of 20 mg/L and adsorbent dosage 1 g/L at different pH values (in the range 2–8). The results are illustrated in Fig. 8(a). From Fig. 8(a), it is clear that the adsorption of Pb(II) on ACS is higher than that of CS, this may be due to the higher surface area of ACS and higher functional groups including acidic hydroxyl, carboxyl, phenolic hydroxyl, and phosphate groups on the ACS surface. The adsorption of Pb(II) ions increases slightly with increasing pH until it reaches the maximum value at pH 5.5, then remains constant until pH 7.1 for both adsorbents. Therefore, pH 5.5 was taken as the optimal value for further adsorption studies. The maximum adsorption capacity of Pb(II) onto CS and ACS is 59.5 and 98.4%, respectively, achieved at pH from 5.5 to 7.1.

The results obtained are discussed according to protonation/deprotonation reactions of the surface functional groups at low and high pH values, respectively. At low pH values, the surface functional groups are protonated and thus the removal percentage of Pb(II) decreased due to charge repulsion. In contrast, at high pH values, the surface functional groups are deprotonated which facilitated the binding of Pb(II) ions with the surface active groups via electrostatic attraction. This can be interpreted according to the species of Pb(II) ions at different pH values, as shown in Fig. 8(b) [29]. It was noticed that, Pb^{2+} is the predominant species at low pH (nearly less than pH 6). At pH from 6 to 7.5, mixture of Pb^{2+} and $\text{Pb}(\text{OH})^+$ are present. While at pH overstep 7.5, $\text{Pb}(\text{OH})^+$ starts to turns to $\text{Pb}_3(\text{OH})_4^{2+}$ and a precipitate of $\text{Pb}(\text{OH})_2$. Thus the adsorption studies for Pb^{2+} ions by CS or ACS were not operated at pH higher than 7.5. Therefore, the effect of pH on the adsorption of Pb(II) on both adsorbents was performed at pH ranges from 2 to 7.1.

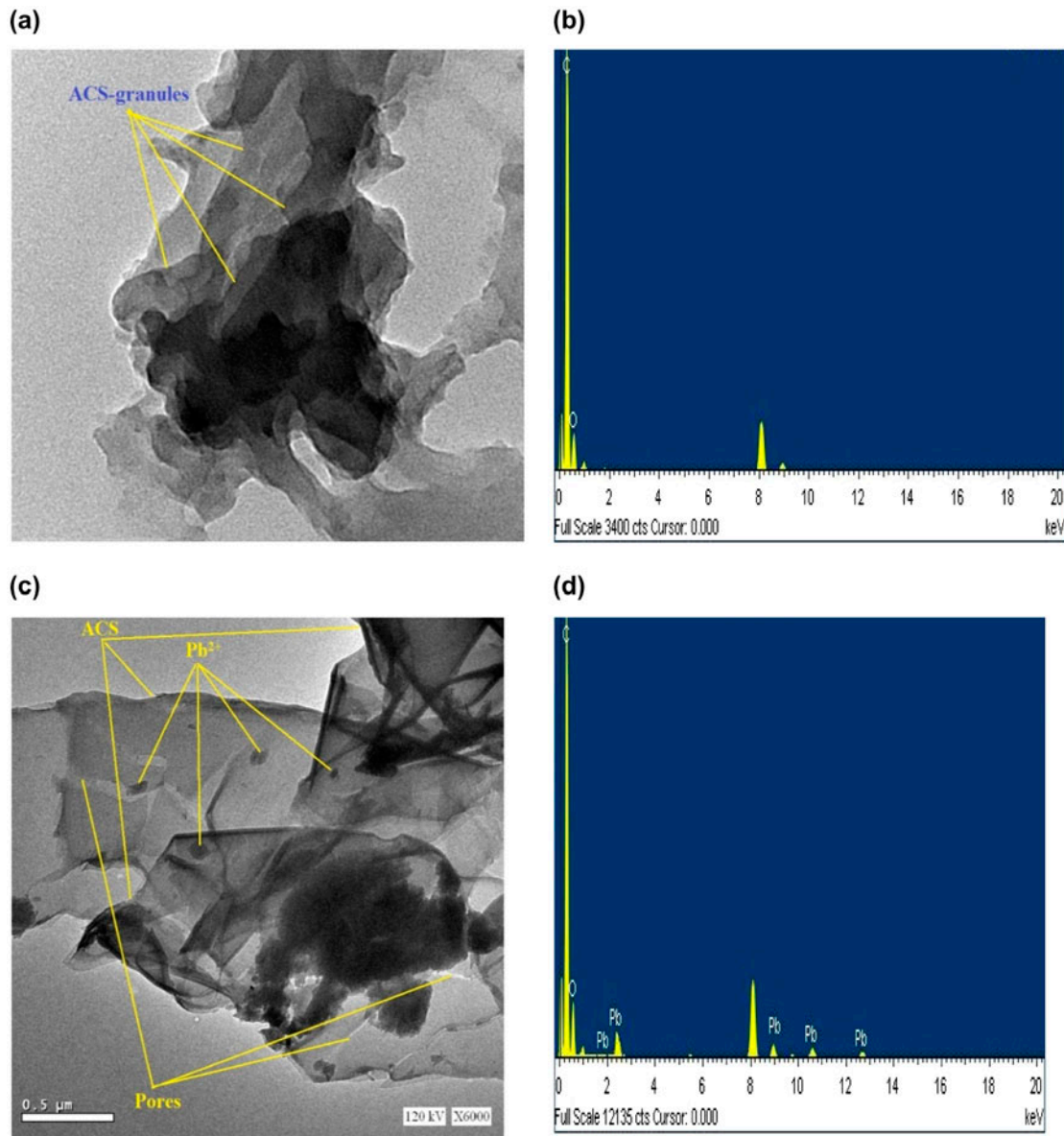


Fig. 5. SEM micrographs ACS before (a) and after (c) adsorbed Pb²⁺, and EDX- of ACS before (b) and after (d) adsorbed Pb²⁺.

Moreover, the pH_{ZPC} values of CS and ACS are nearly 4.2 and 3.3, respectively, as shown in Fig. 6. This means, the surface charge becomes positive at $pH < pH_{ZPC}$ while negative at $pH > pH_{ZPC}$. If the solution pH is lower than pH_{ZPC} , the active sites on the adsorbent surface become inactive for Pb ions adsorption because the adsorbent surface is protonated. However, increasing pH value decreases the protonation of the functional groups on the adsorbent surface and thus enhances Pb(II) adsorption via electrostatic attractions.

However, the only electrostatic attraction could not be ascribed to explain the adsorption of metal cation, but also the surface complexation through ion-exchange process was postulated for enhancing the adsorption of Pb(II) in the range of 2.0–5.5 as $H^+ - Pb^{2+}$ exchange process.

As we know from IR-analysis, the surface of activated carbon contains carboxyl and hydroxyl groups. The ion-exchange mechanism between H^+ ions on the adsorbent surface and metal ion may be described by the following reactions (3, 4) [15,30]:

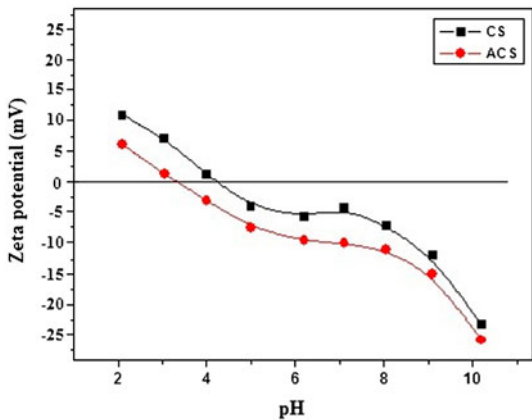


Fig. 6. pH_{ZPC} for the two adsorbents CS and ACS.

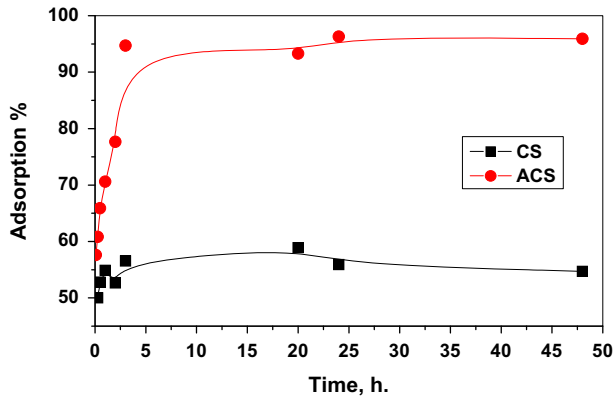


Fig. 7. Effect of time on adsorption of Pb(II) ions on CS and ACS [at pH 5, $C_i = 20 \text{ mg/L}$].



or



where S is the adsorbent surface.

The surface of the two adsorbents (CS and ACS) mainly displays S-OH and S-COOH surface groups [15,30]. The hydroxyl and carboxyl groups at the surface may exchange a proton with positively charged Pb(II) species in aqueous solution forming ion-exchange complex.

This can be confirmed according to: when the pH of solution before ACS or CS adsorbed Pb(II) is 5.5, the pH values of solution after adsorbed Pb(II) were

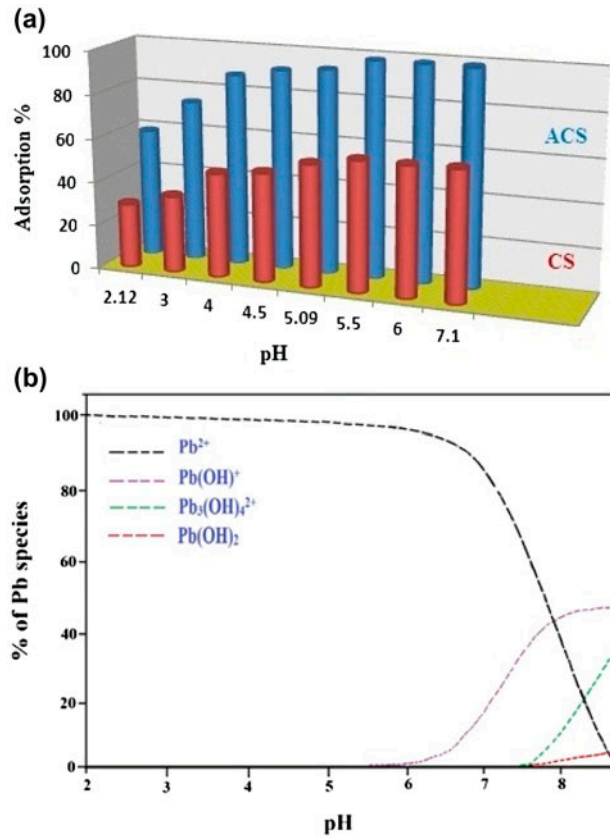


Fig. 8. (a) Effect of pH on adsorption of Pb(II) ions on CS and ACS [at $C_i = 20 \text{ mg/L}$, contact time 3 h] and (b) lead species in aqueous solution as a function of pH.

measured as 4.97 for ACS and 5.20 for CS. This indicated that the pH of solution after Pb(II) adsorption was decreased, which confirm the releasing of H^+ ions in solution, as shown in Eqs. (3) and (4) of ion exchange.

3.2.3. Concentration dependence

The percent removal of lead onto the adsorbents CS and ACS at different initial metal concentrations is shown in Fig. 9. Increasing the initial concentration of Pb(II) leads to decrease in the percent removal of this metal ion. This could be attributed to the fact that at low concentrations, high proportion of active sites on the adsorbent surface is available for the adsorption of metal ions. Subsequently, the percentage of adsorption was optimized at low concentrations. While at high concentrations, the active surface sites on the adsorbents are saturated and covered fully by the adsorbate caused for a decrease in the adsorption percentage of Pb(II) ions [31,32].

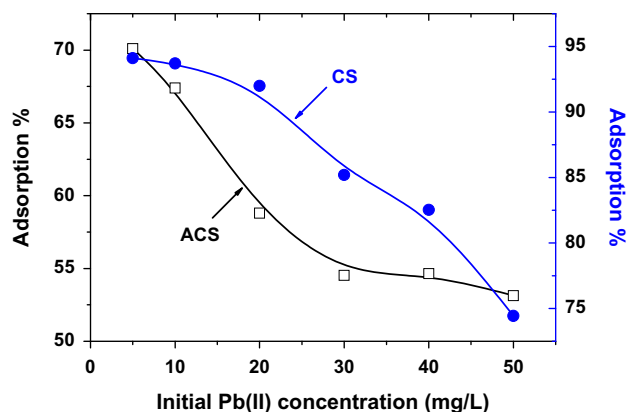


Fig. 9. Effect of initial ion concentration on adsorption of Pb(II) ions on CS and ACS (at pH 5.5, contact time 3 h).

3.2.4. Adsorption isotherms

3.2.4.1. Adsorption isotherm studies using linear form models. The adsorption data that depends on the extent of adsorption with the increase in Pb(II) concentration were analyzed using isotherm models; Freundlich, Langmuir, Temkin, and Dubinin–Radushkevich (D–R) models in linear form and its corresponding isotherm parameters were evaluated.

Langmuir isotherm model demonstrates a monolayer adsorption mechanism with homogeneous adsorption energies and is described by the following Eq. (5) [33]:

$$\frac{1}{q_e} = \frac{1}{q_{mL}} + \left(\frac{1}{K_L q_{mL}} \right) \left(\frac{1}{C_e} \right) \quad (5)$$

where q_{mL} and K_L are Langmuir constants related to monolayer adsorption capacity (mg/g) and adsorption energy (L/mg), respectively.

Freundlich isotherm model describes the multilayer adsorption of lead ions on the adsorbent surface with heterogeneous surface energy and is expressed in the linear form as (Eq. (6)) [34]:

$$\log q_e = \log K_F + \left(\frac{1}{n_F} \right) \log C_e \quad (6)$$

where q_e (mg/g) is the amount of Pb(II) ions adsorbed per gram of adsorbent at equilibrium, C_e (mg/L) is the equilibrium concentration of Pb(II) ions remained in the solution, K_F and $1/n_F$ are Freundlich constants that can be related to the adsorption capacity of the adsorbent ((mg/g)(L/mg)^{1/n}) and the intensity of adsorption, respectively.

Temkin isotherm model assumes that the heat of adsorption of ions in the layer decreases linearly with coverage, which is due to the adsorbate and adsorbate interactions. Temkin model is given by (Eq. (7)) [35]:

$$q_e = \left(\frac{RT}{b} \right) \ln K_T + \left(\frac{RT}{b} \right) \ln C_e; \quad \delta_T = \frac{RT}{b} \quad (7)$$

where b is the Temkin constant (J/mol) related to the adsorption heat, T is the absolute temperature (K), R is the gas constant (8.314 J/mol K), and K_T is the Temkin isotherm constant (L/g).

Dubinin–Radushkevich (D–R) isotherm model is applied to identify the nature of adsorption processes. The linear form of D–R isotherm equation is given by Eq. (8) [36]:

$$\ln q_e = \ln q_{DR} - K_{DR} \varepsilon^2 \quad (8)$$

where q_e is the adsorption capacity (mol/g), q_{DR} is the maximum adsorption capacity, i.e. the amount of metal ions at complete monolayer coverage (mol/g), K_{DR} is the parameter related to the adsorption energy (mol²/kJ²) and ε is the Polanyi potential ($\varepsilon = RT \ln(1 + 1/C_e)$). The value of K_{DR} is related to the adsorption energy, E (kJ/mol), which is defined as the free energy change required to transfer a molecule from solution to the solid surfaces. The adsorption energy can be calculated by Eq. (9):

$$E = \frac{1}{\sqrt{2K_{DR}}} \quad (9)$$

A plot of $\ln q_e$ vs. ε^2 will give the values of K_{DR} and q_{DR} from the slope and intercept.

The adsorption energy, E , gives information about adsorption mechanism as chemical ion-exchange or physical adsorption. If E value < 8 kJ/mol, the adsorption is physical in nature, whereas, if $8 < E < 16$ kJ/mol, the ion exchange is the adsorption mechanism, while if $E > 16$ kJ/mol, the chemical adsorption occur [17]. The calculated E values for Pb (II) adsorption onto CS and ACS are lower than 8 kJ/mol, thereby suggesting that the adsorption process may be carried out via physical adsorption.

The plots presentation of the adsorption isotherms of Pb(II) ions onto CS and ACS are illustrated in Fig. 10. The values of isotherm constants and the correlation coefficients (R^2) are presented in Table 2. The standard deviation (SD) and the statistical errors as the residual sum of square error (RSSE) and the root mean square error (RMSE) are also placed in Table 2

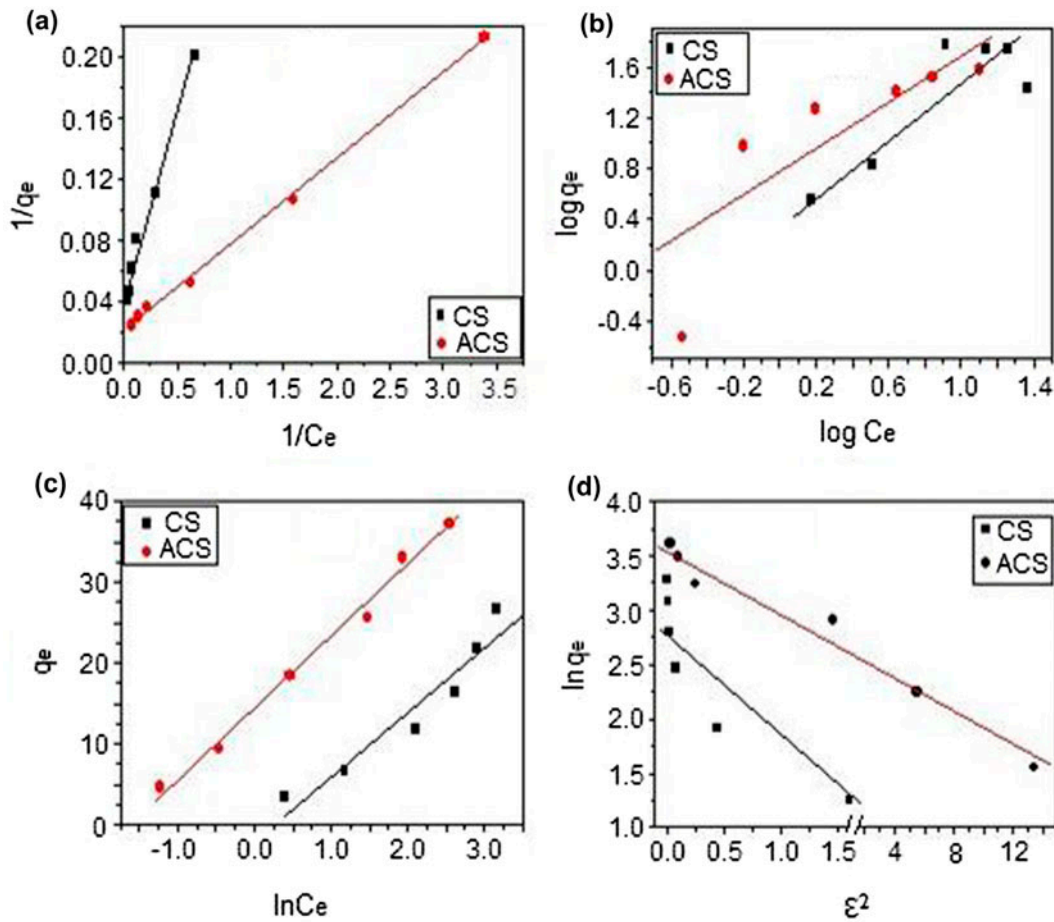


Fig. 10. (a) Langmuir, (b) Freundlich (c) Temkin, and (d) D–R isotherms for adsorption of Pb(II) ions onto CS and ACS.

and calculated according to Eqs. (10)–(12) as follow [37–39]:

$$SD = 100 \times \sqrt{\frac{\sum [(q_t^{\text{exp}} - q_t^{\text{cal}}) / q_t^{\text{exp}}]^2}{N - 1}} \quad (10)$$

$$RSSE = \sum_{i=1}^{N_e} (q_{\text{exp}} - q_{\text{cal}})^2 \quad (11)$$

$$RMSE = \sqrt{N_e \sum_{i=1}^{N_e} \left[\frac{(q_{\text{exp}} - q_{\text{cal}})^2}{N_e} \right]} \quad (12)$$

where q_t^{exp} and q_t^{cal} are the amounts of Pb(II) adsorbed experimentally and calculated from the model at time t , respectively, N_e is the number of experimental data points, and e is the number of parameters in the model. A model is considered as good if the

correlation coefficient (R^2) is high, and all statistical errors and SD are minimum.

From Table 2, it was observed that the Langmuir isotherm model has higher correlation coefficient (R^2) and lower in SD, RMSE, and RSSE when compared to the other models. Where R^2 for adsorption of Pb(II) ions onto ACS are 0.99924, 0.84716, 0.99503, and 0.95671 and onto CS are 0.99178, 0.85905, 0.95637, and 0.89431 for Langmuir, Freundlich, Temkin, and D–R isotherm models, respectively. Also, SD, root of mean square error (RMSE) and the residual of sum of square error (RSSE) of Langmuir model for ACS are 0.00319, 1.016×10^{-5} , and 4.065×10^{-5} and for CS are 0.00855, 7.311×10^{-5} and 2.924×10^{-4} , respectively, which are lower than that for the other models. Thus the isotherm data follow the Langmuir model. Therefore, the adsorption process of Pb(II) onto CS and ACS follows the Langmuir isotherm model, indicating a monolayer adsorption sites with homogeneous nature of the adsorbent without any interaction between adsorbed molecules [40].

Table 2
Isotherm constants for adsorption of Pb(II) onto CS and ACS for linear models

Isotherm models	Parameters	Values for CS	Values for ACS
Langmuir	q_{\max} (mg/g)	26.14	49.92
	b (L/mg)	0.15761	0.35558
	R^2	0.99178	0.99924
	SD	0.00855	0.00319
	RMSE	7.311×10^{-5}	1.016×10^{-5}
	RSSE	2.924×10^{-4}	4.065×10^{-5}
Freundlich	k (mg/g)(L/mg) $^{1/n}$	2.91781	4.63701
	n	1.02201	0.93911
	R^2	0.85905	0.84716
	SD	0.30294	0.47271
	RMSE	0.09177	0.22345
	RSSE	0.36709	0.89382
Temkin	A (L/g)	0.99417	5.09851
	b (kJ/mol)	0.31317	0.28093
	R^2	0.95637	0.99503
	SD	2.89196	1.43851
	RMSE	8.36344	2.06931
	RSSE	33.4537	8.27721
D-R	q_m	17.46205	28.35207
	k (mol 2 /kJ 2)	1.0844×10^{-6}	0.1448×10^{-6}
	E (kJ/mol)	0.67902	1.85829
	R^2	0.89431	0.95671
	SD	0.38313	0.26163
	RSSE	0.14679	0.06845

The prepared ACS displayed higher sorption capacity (49.92 mg/g) than that for CS (26.14 mg/g). This may be due to higher surface area, higher active sites, and large pore volumes for ACS than CS, which causes higher sorption process [41]. In addition, the radius of Pb(II) ion is 0.119 nm (Pb diameter equal about 0.24 nm), which Pb(II) ions easily enter inside the micropores (<2 nm) of the adsorbent surface. Therefore, the higher micropores percent for ACS than that for CS, as shown in Table 1, led to increase the adsorption capacity for Pb(II) ions.

Modified CS was also previously used as activated carbon for removal of lead ions. Sekar et al. reported that, the adsorption capacity of Pb(II) onto activated carbon prepared from coconut shell using concentrated H₂SO₄ reached 12.64 mg/g at 20 mg/L Pb(II) concentration [30]. Also Song et al. indicated that the adsorption capacity of Pb(II) onto activated carbon prepared from CS using HCl (2 mol L⁻¹) (denoted as AC0), oxidation of sample AC0 with 10 mol L⁻¹ H₂O₂ at room temperature, and at 363 K for 24 h (samples

labeled as AC1 and AC2, respectively), oxidation of sample AC0 with 10 mol L⁻¹ HNO₃ at room temperature and at 363 K for 4 h (samples labeled as AC3 and AC4, respectively) and with 5 mol L⁻¹ HNO₃ at 363 K for 4 h (labeled as AC5) were 17.193, 22.792, 28.458, 25.197, 40.119, and 37.938 mg/g onto AC0, AC1, AC2, AC3, AC4, and AC5, respectively [42]. In this study, the maximum adsorption capacity obtained for chemically activated CS using H₃PO₄ from Langmuir isotherm was 49.92 mg/g for Pb(II) ions.

The dimensionless separation factor (R_L), defined by Eq. (13) [2], is an important characteristic of Langmuir isotherm. This factor explains the nature of the adsorption process on the adsorbent ($R_L > 1$, unfavorable; $R_L = 1$, linear; $0 < R_L < 1$, favorable; and $R_L > 0$, irreversible):

$$R_L = \frac{1}{1 + bC_0} \quad (13)$$

where C_0 is the initial Pb(II) concentration (mg/L) and b is the Langmuir constant (L/g).

R_L values were calculated from the entire concentration range studied and presented in Table 3. From this table, it shows that the value of separation factor (R_L) is greater than 0 and less than 1 for CS and ACS, indicating favorable adsorption.

3.2.4.2. Adsorption isotherm studies using nonlinear form models. It is fundamentally required to analyze the experimental isotherm data of Pb(II) adsorption onto two activated carbons using nonlinear isotherm models. These models are: two-parameter isotherm models namely, Langmuir (Eq. (14)), Freundlich (Eq. (15)), Temkin (Eq. (16)), and D–R (Eq. (17)) models. The fitting of these models are shown in Fig. 11. The three-parameter isotherm models are namely, Generalized (Eq. (18)) [43], Toth (Eq. (19)) [43], Radke–Prausnitz (Eq. (20)) [44], and Fritz–Schlunder (Eq. (21)) [45] models. The nonlinearized forms of these isotherm models are given as follows:

$$q_e = \frac{q_{mL} K_L C_e}{1 + K_L C_e} \quad (14)$$

$$q_e = K_F C_e^{1/N_F} \quad (15)$$

$$q_e = \delta_T \ln K_T + \delta_T \ln C_e \quad (16)$$

$$q_e = q_{DR} \exp(-K_{DR} RT \ln(1 + 1/C_e)); \quad E = \frac{1}{\sqrt{2} K_{DR}} \quad (17)$$

$$q_e = \frac{q_{mG} C_e^{N_G}}{K_G + C_e^{N_G}} \quad (18)$$

$$q_e = \frac{q_{mT} C_e}{(B_T + C_e^{N_T})^{1/N_T}} \quad (19)$$

Table 3

Different values of R_L at different concentrations of Pb(II) onto CS and ACS

C_0	R_L for CS	R_L for ACS
5	0.55926	0.35998
10	0.38818	0.21950
20	0.24084	0.12328
30	0.17457	0.08571
40	0.13690	0.06568
50	0.11261	0.05325

$$\frac{1}{q_e} = \frac{1}{K_{RP} C_e} + \frac{1}{\beta C_e^{1/P}} \quad (20)$$

$$q_e = \frac{q_{mF} K_F C_e}{1 + q_{mF} C_e^\alpha} \quad (21)$$

where q_e is the amount of Pb(II) adsorbed onto the adsorbent at equilibrium (mg/g), C_e is the concentration of adsorbate on adsorbent at equilibrium (mg/L), q_{mL} , q_{mG} , q_{mT} , and q_{mF} are the maximum adsorption capacity (mg/g) of Langmuir, Generalized, Toth, and Fritz–Schlunder, respectively. N_G , B_T , K_{RP} , K_F , and K_G , N_T , p , α are the Generalized, Toth, Radke–Prausnitz, and Fritz–Schlunder equilibrium constants and the models exponents. β is the Radke–Prausnitz constant. The parameters of the Langmuir, Freundlich, Temkin, and D–R models were defined previously. The parameters of all models are calculated by nonlinear fitting of the experimental adsorption equilibrium data using Origin Pro 8.5 software, and they are shown in Table 4. The correlation coefficient values (R^2), the RSSE, and the RMSE values are also listed in Table 4 to distinguish between the investigated models. The higher R^2 values for the two-parameters and the three-parameters represent that the adsorption data of Pb(II) on the synthetic activated carbons are well depicted by these models. The best isotherm model was chosen according to the lower values of RSSE and RMSE and higher values of the correlation coefficient (R^2).

According to the values of RSSE and RMSE that are shown in Table 4, for adsorption of Pb(II) onto CS-adsorbent, it was noticed that the three-parameter isotherm models have lower error values than that for the two-parameters isotherm models except for the nonlinear Freundlich model, which has lower RSSE and RMSE values. Therefore, this suggests that the applicability of the three-parameter isotherm models and the Freundlich nonlinear model for performing the experimental isotherm data of Pb(II) adsorbed on the CS is greater than the other two-parameter isotherm models. For the two-parameter models, according to the R^2 , RSSE and RMSE-values, the adsorption equilibrium data can be represented well with the Freundlich model, and this means highly heterogeneous CS-surfaces. The three-parameter models can be present in the following order of fitness: (1) based on the maximum adsorption capacity: Generalized > Fritz–Schlunder > Toth, which confirm the maximum capacity value of Langmuir model of linear form, (2) based on the correlation coefficient, RSSE and RMSE-values: Fritz–Schlunder > Radke–Prausnitz > Toth > Generalized.

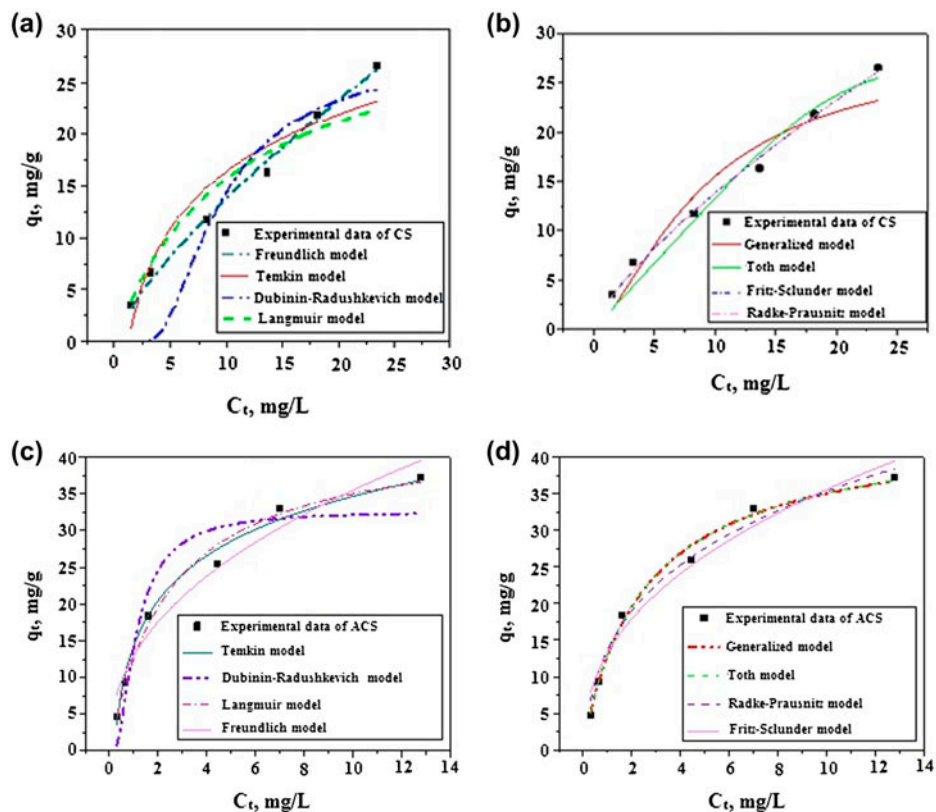


Fig. 11. Langmuir, Freundlich, Temkin, and Dubinin–Radushkevich nonlinear models of (a) CS and (c) ACS. Generalized, Toth, Radke–Prausnitz, and Fritz–Schlunder nonlinear models of (b) CS and (d) ACS.

For adsorption of Pb(II) onto ACS-adsorbent, the experimental data were also analyzed using the last eight nonlinear models. The models fit for the two-parameter and for the three-parameter isotherms along with experimental data are present in Fig. 11(c) and (d), respectively. The values of the models parameters along with the R^2 , RSSE, and RMSE values are present in Table 4. It was noticed that for the two-parameter models, Langmuir and Temkin models were found to obey the experimental data in acceptable values of $R^2 = 0.98637$, RSSE = 9.10, and RMSE = 2.27 for Langmuir model and $R^2 = 0.98743$, RSSE = 8.39, and RMSE = 2.09 for Temkin model. In addition, the maximum adsorption capacity value for adsorption of lead onto the ACS from the nonlinear Langmuir model was matched with that obtained from the Langmuir linear model. In addition, the three parameter models are fit well the experimental data according to the correlation coefficient, RSSE and RMSE-values in the order: Toth > Generalized > Radke–Prausnitz > Fritz–Schlunder. Based on the maximum adsorption capacity, the fitness order follows: Toth > Generalized > Fritz–Schlunder and the obtained values of the

maximum adsorption capacities agree with that obtained from the Langmuir linear model. Generally, the adsorption capacities for adsorption of Pb(II) on ACS are higher than that obtained from the models in case of CS. This means, ACS is more suitable than CS for adsorption of Pb(II).

Table 5 shows a comparison between the sorption capacities of the adsorbents (CS and ACS) used in this work with other adsorbents reported in literature [8,12,14,46–55]. As can be seen from Table 5, ACS has the higher adsorption capacity than that for others, which is the highest capacity in this series. Thus, ACS is the most effective for the removal of Pb(II) from aqueous solution.

3.2.5. Kinetic studies

Different adsorption kinetic models, such as pseudo-first-order, pseudo-second-order, Elovich, and mass transfer diffusion models (Mathews–Weber, Bangham’s, Vermeulen’s, and Weber–Morris’s diffusion models) were applied to describe the contact time’s experimental data.

Table 4
Isotherm constants for adsorption of Pb(II) onto CS and ACS for nonlinear models

Isotherm models	Parameters	Values for CS	Values for ACS
<i>Nonlinear model in two unknown parameters</i>			
Langmuir	q_{mL}	32.6001	43.5818
	K_L	0.09288	0.40831
	R^2	0.92371	0.98637
	RMSE	5.98023	2.27502
	RSSE	29.90117	9.10006
Freundlich	K_F	2.44934	13
	N_F	1.33121	2.29195
	R^2	0.99339	0.96558
	RMSE	0.51806	5.74567
	RSSE	2.07222	28.72833
Temkin	K_T	313.17008	5.09842
	δ_T	0.79362	280.99419
	R^2	0.89331	0.98743
	RMSE	8.36308	2.09882
	RSSE	33.45232	8.39527
D-R	q_{DR}	27.47234	32.62384
	k_{DR}	0.02871	6.91014×10^{-4}
	R^2	0.77583	0.87633
	RMSE	17.57138	20.64281
	RSSE	70.28552	82.57124
<i>Nonlinear model in three unknown parameters</i>			
Generalized	q_{mG}	29	45
	N_G	1.47086	0.94025
	k_G	25.6839	2.47788
	R^2	0.92151	0.99107
	RMSE	6.15304	1.49828
	RSSE	24.6121	5.99314
Toth	q_{mT}	27.5	46
	B_T	1.57401×10^7	2.04155
	N_T	5.46864	0.87896
	R^2	0.96076	0.99143
	RMSE	3.07561	1.43708
	RSSE	12.3024	5.74833
Radke–Prausnitz	k_{RP}	27.8	45.8
	β	2.65206	19.6423
	P	1.35328	3.44862
	R^2	0.99322	0.98089
	RMSE	0.53117	12.8179
	RSSE	2.12468	1.65739
Fritz–Schlunder	q_{mF}	28.1	44.3
	k_F	2.52554	13.5991
	α	0.25351	0.57977
	R^2	0.99333	0.95842
	RMSE	0.52301	6.97489
	RSSE	2.09202	27.8995

Table 5
Comparison of maximum adsorption capacities of Pb(II) by various adsorbents

Adsorbent	q_{\max} (mg/g) (from Langmuir)	pH	Adsorbent dosage (g/L)	Refs.
ACS	49.92	5.5	1	This study
CS	26.14	5.5	1	This study
Activated carbon from coconut (CA)	4.38	4	120	[46]
Graphite	2.2	–	1.6	[47]
GO	30.1	–	1.6	[47]
A.C. from Apricot stone	21.38	6	1	[14]
Pine cone A.C.	27.53	5.2	2	[12]
Magnetic ion-imprinted and –SH functionalized polymer (Fe ₃ O ₄ @SiO ₂ -IIP)	32.58	6–7	1	[48]
The magnetic nonimprinted polymer (Fe ₃ O ₄ @SiO ₂ -NIP)	16.50	6–7	1	[48]
ASG (activated silica gel)	15.62	5.5	2	[49]
TLSG (thiophenecarbonyl loaded silica gel)	17.85	5.5	2	[49]
FLSG (2-furoyl loaded silica gel)	19.60	5.5	22	[49]
PLSG (L-Proline loaded silica gel)	22.22	5.5	2	[49]
MT (mechanically treated newspaper pulp)	19.01	6	2	[50]
CA-modified 0.5 M	25.71	6	2	[50]
CA-modified 1 M	34.60	6	2	[50]
Soil	20.157	4.5	5	[51]
ZnO	26.10	2 or 4	10 or 4	[52]
Calcium chloride-treated U. fasciata carbon (CCUC)	29.93	4	2	[53]
Sodium sulfate-treated U. fasciata carbon (SSUC)	24.154	4	2	[53]
Sodium carbonate-treated U. fasciata carbon (SCUC)	23.47	4	2	[53]
Commercially activated carbon (CAC)	15.62	4	2	[53]
PAN-ACFs	36.6	4	7.5	[54]
A.C. from date stones	38.64	6	–	[55]
EDTA-Zr(IV) iodate	26.04	6	10	[8]

The linear form of pseudo-first-order (Lagergren equation) and pseudo-second-order kinetic models are expressed as Eqs. (22) and (23), respectively [56,57]:

$$\log(q_e - q_t) = \log q_e - \frac{k_1}{2.303} t \quad (22)$$

$$\frac{t}{q_t} = \frac{1}{k_2 q_e^2} + \frac{t}{q_e} \quad (23)$$

where k_1 (1/min) and k_2 (g/mg min) are the first-order and second-order rate constants, respectively. q_e and q_t are the amounts of metal ion adsorbed (mg/g) on the adsorbents at equilibrium and at time t , respectively. The values of parameters q_e , k_1 and k_2 are calculated from the intercept and slope of these plots (Fig. 12(a) and (b)) and presented in Table 6. From Table 6, it can be seen that the calculated q_e values from pseudo-second-order agree very well with the experimental values and the correlation coefficients for CS and ACS

($R^2 = 0.99877$ and 0.99975 , respectively) are better than for the pseudo-first-order kinetic model ($R^2 = 0.78458$ for CS and 0.90718 for ACS). Therefore, the adsorption kinetics of Pb(II) onto CS and ACS are described by a pseudo-second-order model. Pseudo-second-order kinetic model indicated that the prevailing process is chemisorption, through sharing of electrons between the adsorbate and the adsorbent surface [58]. In addition, the value of k_1 (0.9592) of ACS is higher than of CS (0.35075). This result confirms the better sorption capacity of ACS and this reason agrees with the literature [46].

The Elovich kinetic model supposes that the adsorbent surface is heterogeneous in nature [59]. This model is described by the following equation (Eq. (24)) [60]:

$$q_t = \frac{1}{\beta} \ln(\alpha \beta) + \frac{1}{\beta} \ln(t) \quad (24)$$

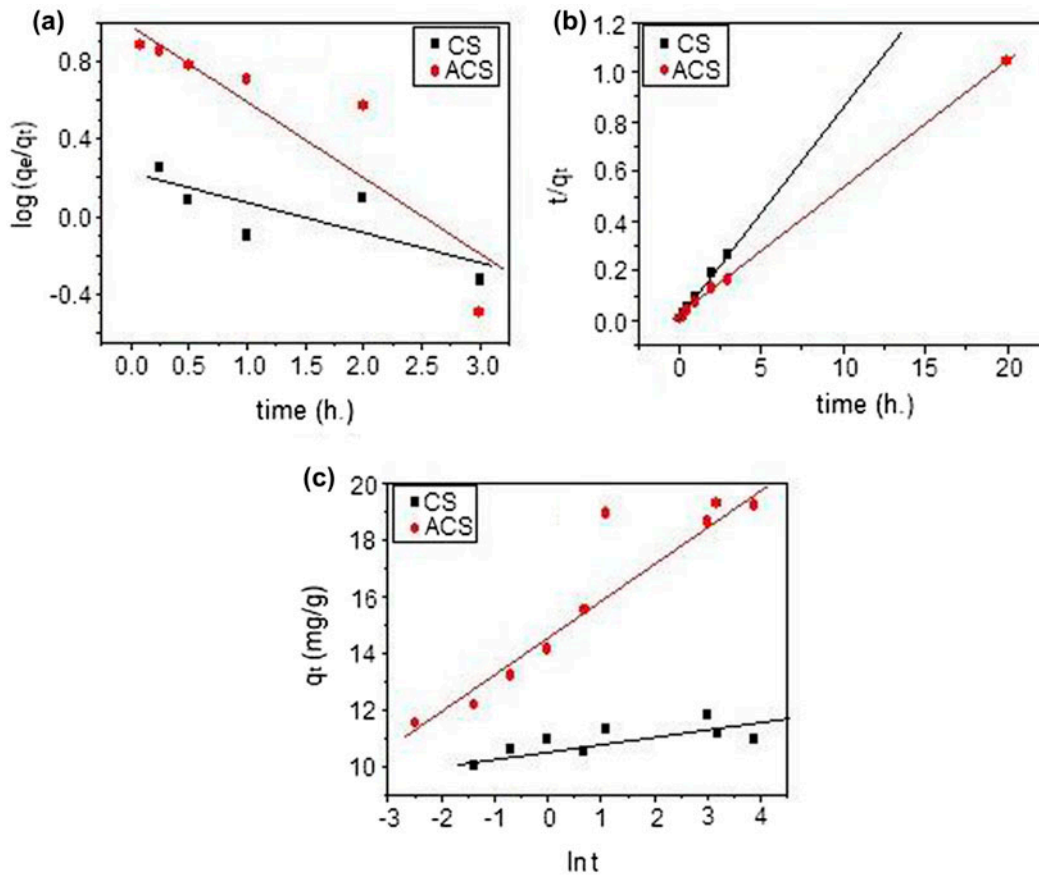


Fig. 12. (a) Pseudo-first-order, (b) pseudo-second-order, and (c) Elovich models for adsorption of Pb(II) ions onto CS and ACS.

where α (mg/g min) and β (g/mg) are the Elovich parameters defined as the initial adsorption rate and the desorption constant, related to the degree of surface coverage, respectively.

The plot of q_t vs. $\ln(t)$ is indicated in Fig. 12(c) and the kinetic constants α and β are calculated from the slope and the intercept. The obtained values and the correlation coefficient (R^2), SD, the RSSE, and the RMSE are presented in Table 6.

From Table 6, the correlation coefficient (R^2) values of Elovich model are lower than that of Pseudo-second-order, indicating that the kinetic data does not fit with the Elovich kinetic model. Errors and SD values as shown in Table 6 are also considerably less for Pseudo-second-order kinetic model than Pseudo-first-order and Elovich model, reinforcing the applicability of the Pseudo-second-order kinetic model.

3.2.5.1. Mass transfer diffusion studies. Different diffusion models were used to describe the mechanism of solid-solute adsorption process, through identification of the rate determining step. The adsorption of Pb

(II) from aqueous solution on the adsorbents depends on three steps; the first step, transport of the adsorbate molecules from the bulk solution to the external surface of the adsorbent by diffusion through the boundary layer. The second step, transport of the adsorbate within the pores of the adsorbent, and the third step indicates adsorption of the adsorbate onto the adsorbent surface. To determine the diffusion of Pb(II) ions on CS and ACS as adsorbents, the kinetic results were further analyzed by different four diffusion models.

3.2.5.2. Mathews–Weber diffusion model. This model is used to examine the external mass transfer on the fluid boundary phase around the solid particles, which is defined as follows [61]:

$$\log \frac{C_t}{C_0} = \left(-\frac{K_m \cdot A}{2.303} \right) t \quad (25)$$

Table 6
Kinetic model parameters for adsorption of Pb(II) onto CS and ACS

Kinetic models	Parameters	Values for CS	Values for ACS
Pseudo-first-order	q_e^{exp} (mg/g)	11.78	19.26
	q_e^{cal} (mg/g)	1.61312	10.6241
	k_1 (1/min)	0.35075	0.95921
	R^2	0.78458	0.90718
	SD	0.15867	0.24697
	RMSE	0.02517	0.06099
	RSSE	0.07552	0.24397
Pseudo-second-order	q_e^{cal} (mg/g)	11.2676	19.4099
	k_2 (g/mg min)	2.01452	0.22381
	R^2	0.99877	0.99975
	SD	0.00581	0.00905
	RMSE	3.317×10^{-5}	8.197×10^{-5}
	RSSE	1.979×10^{-4}	9.861×10^{-4}
Elovich model	α (mg/g min)	2.597×10^{22}	5.884×10^4
	β (g/mg)	4.98977	0.72398
	R^2	0.71014	0.94183
	SD	0.41559	1.15551
	RMSE	0.17272	1.33518
	RSSE	1.03631	9.34627
Mathews–Weber model	$K_M A$ (h ⁻¹)	0.05501	0.63722
	Intercept	-0.29579	-0.30204
	R^2	0.80081	0.84881
	SD	0.01331	0.13121
	RMSE	1.76806×10^{-4}	0.01722
	RSSE	7.07225×10^{-4}	0.06887
Bangham's model	K_B (mL/g L)	0.01061	0.01461
	θ	0.05831	0.11881
	R^2	0.99394	0.98166
	SD	0.00265	0.00943
	RMSE	7.01163×10^{-6}	8.89237×10^{-5}
	RSSE	2.80465×10^{-5}	3.55695×10^{-4}
Vermeulen's model	K_V	0.42944	0.77345
	Intercept	1.22861	0.22663
	R^2	0.95346	0.93401
	SD	0.10796	0.23343
	RMSE	0.01165	0.05449
	RSSE	0.04662	0.21796
Weber–Morris model	K_{Wm} (mg/g min ^{0.5})	1.92509	3.60578
	C (mg/g)	9.09705	10.4823
	R^2	0.98366	0.99796
	SD	0.12521	0.11731
	RMSE	0.01567	0.01376
	RSSE	0.01567	0.04128

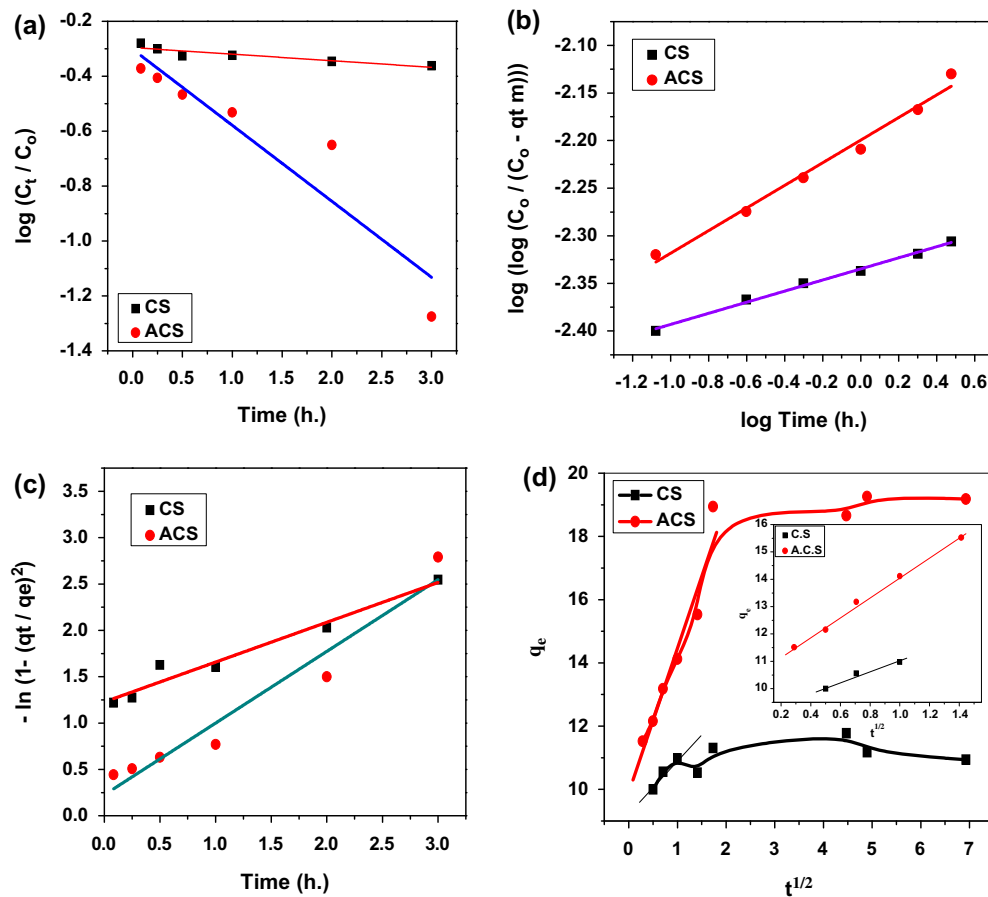


Fig. 13. (a) Mathews–Weber, (b) Bangham’s, (c) Vermeulen’s, and (d) Weber–Morris’s diffusion models.

where C_t and C_0 are the adsorbate concentration at time t and the initial solute concentration (mg/g), respectively. K_m is the external mass transfer coefficient (m h^{-1}) and A is the external surface per unit mass (m^2/g).

The Mathews–Weber is confirmed, if the linear plot of $\log(C_t/C_0)$ vs. t is passing through the origin, which the kinetic mechanism is controlled by external mass transfer. At this work, the plot of Mathews–Weber model for adsorption of Pb(II) ions on the two adsorbents CS and ACS is shown in Fig. 13(a) and the values of the volumetric mass transfer coefficient as well as the intercept, the correlation coefficient and the residual sum of square and the RMSEs were tabulated in Table 6. As noticed from the Fig. 13(a) and Table 6, the linear plot for both adsorbents are not passing the origin with intercept values and low R^2 values. This means, the diffusion of Pb(II) ions on the two adsorbents CS and ACS is not defined by the fluid film diffusion.

3.2.5.3. *Bangham’s diffusion model.* This model is employed to determine if the rate limiting step is controlled by the pore diffusion only or not. The Bangham model is given as [62]:

$$\log \left[\log \left(\frac{C_0}{C_0 - q_t m} \right) \right] = \log \left(\frac{K_B m}{2.303 V} \right) + \theta \log t \quad (26)$$

where V is the volume of liquid phase (ml), m is the weight of adsorbent per liter of solution (g/L), and K_B and θ (<1) are constants. K_B and θ were calculated from the intercept and the slope of the straight line plots of $\log[\log(C_0/C_0 - q_t m)]$ against $\log t$ (Fig. 13(b)), respectively. Table 6 lists the Bangham’s parameters as well as the R^2 , RSSE, and MSE values.

The Bangham’s plot gives straight lines not only with higher R^2 -values, but also with very lower RSSE and RMSE errors for both studied adsorbents. This indicates that the Bangham’s model is applicable, and

the rate determining step for adsorption of Pb(II) ions is mainly controlled by pore diffusion for the two adsorbents CS and ACS.

3.2.5.4. *Vermeulen’s diffusion model.* If the adsorbate diffusion through the adsorbent beads is the slowest step, the particle diffusion will be the rate determining step. The model was expressed by the following expression [63,64]:

$$-\ln\left[1 - \left(\frac{q_t}{q_e}\right)^2\right] = \left(\frac{2\pi^2 D_v}{r_0^2}\right)t = K_v t \tag{27}$$

where D_v is the effective diffusion coefficient, r_0^2 is the radius of the adsorbent particles supposed to spherical particles, q_t/q_e is the fraction realization of equilibrium at time t .

When the plot of $-\ln[1 - (q_t/q_e)^2]$ vs. t give straight line passing through the origin, Vermeulen’s model is applicable for these kinetic data. The vermeulen’s plot for adsorption of Pb(II) onto CS and ACS adsorbents

was cleared at Fig. 13(c). The values of K_v , intercept, R^2 and errors are calculated and illustrated in Table 6. As shown from Fig. 13(c) and Table 6, the Vermeulen’ plot did not yield satisfactory linear curves for both adsorbents where low R^2 values were obtained ($R^2 = 0.95346$ and 0.93401 for CS and ACS, respectively). This means the diffusion of lead(II) through the adsorbent beads is not the rate-controlling step.

3.2.5.5. *Weber–Morris’s diffusion model.* To predict the rate determining step in the adsorption process of Pb (II), Weber and Morris equation (Eq. (28)) was used as follows [58]:

$$q_t = k_{Wm}t^{1/2} + C \tag{28}$$

where k_{Wm} (mg/g min^{0.5}) is the intra-particle diffusion rate constant and C (mg/g) is proportional to the boundary layer thickness. The constants k_{Wm} and C are obtained from the slope and intercept of the straight line of q_t vs. $t^{1/2}$ (Fig. 13(d)) and listed in

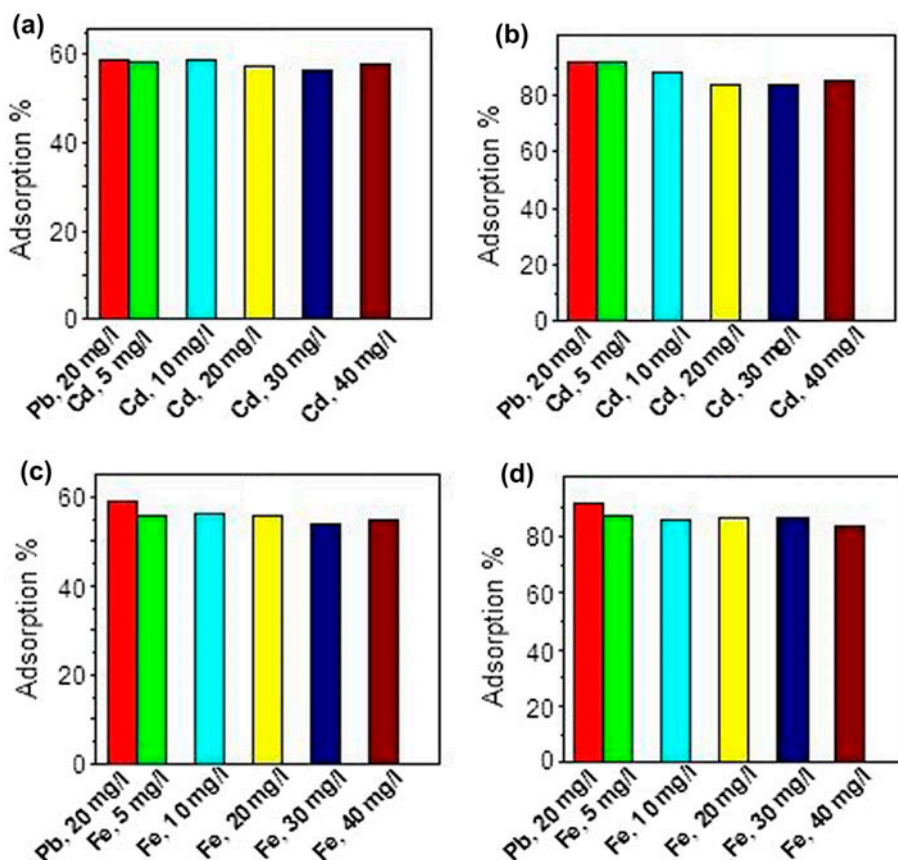


Fig. 14. Effect of competing ions (a and b) Pb(II) with Cd(II) on CS and ACS, respectively, and (c and d) Pb(II) with Fe (III) on CS and ACS, respectively.

Table 6. Ho [65] demonstrated that the intra-particle diffusion is the rate limiting step, when the plot passes through the origin (i.e. $C = 0.0$). If the value of C is higher than zero, difference in the rate of mass transfer during initial and final stages occurred. It can be seen from Fig. 13(d) that the plot do not path through the origin (the value of $C > 0$), hence the mechanism of the adsorption process is probably a combination of boundary layer and pore diffusion which contribute to the rate determining step [66]. Therefore, the adsorption of Pb(II) ions onto CS and ACS surface is a complex, involving more than one mechanism as shown in Fig. 1.

3.2.6. Effect of competing ions

The existence of other ions in the solution may reduce the adsorption process of the given adsorbate to some extent. Thus the presence of Cd(II) with Pb(II) and Fe(III) with Pb(II) were chosen for study and the results are shown in Fig. 14. It pointed out that the effect of Cd(II) and Fe(III) on the adsorption of Pb(II) was considerably feeble, even with increasing the ions concentration. Which means that they do not compete for the active sites with Pb(II) [67]. This may be due to Pb having a large ionic radii and is more electronegative (0.120 nm and 2.33, respectively) than Cd (0.097 nm and 1.69) and Fe (0.064 nm and 1.83), indicating that Pb has higher adsorption on both CS and ACS according to Zhang et al. and Suzuki et al. [2,68].

4. Conclusion

In this study, CS chemically activated by phosphoric acid (ACS) was used as a good adsorbent for removal of Pb(II) ion from aqueous solution. ACS has higher efficiency for sorption of Pb(II) ions than the pyrolysis CS, and the percent removal was found 98.4 and 59.5% for ACS and CS, respectively. The optimum pH and contact time was found to be 5.5 and 3 h. The equilibrium adsorption data indicated best fit to the Langmuir isotherm model and the maximum monolayer adsorption capacity, q_{max} , was found to be 49.92 mg/g, and this matched with the result obtained from the nonlinear isotherm models. The values of the separation factor R_L pointed out that the adsorption process is favorable for Pb(II) adsorption onto ACS. It was found that the kinetic adsorption follows very well the pseudo-second-order model, indicating the chemisorption. The adsorption process seems to be affected by both boundary layer and pore diffusion. The results show that, ACS has higher affinity for removal of the Pb(II) ions in the presence of high

concentration of Cd(II) or Fe(III) ions. Therefore, the coconut shell activated carbon (ACS) can be effectively applied as a good adsorbent for removal of Pb(II) ions from aqueous solution.

References

- [1] S.K. Yadav, D.K. Singh, S. Sinha, Chemical carbonization of papaya seed originated charcoals for sorption of Pb(II) from aqueous solution, *J. Environ. Chem. Eng.* 2 (2014) 9–19.
- [2] Z. Zhang, M. Li, W. Chen, S. Zhu, N. Liu, L. Zhu, Immobilization of lead and cadmium from aqueous solution and contaminated sediment using nano-hydroxyapatite, *Environ. Pollut.* 158 (2010) 514–519.
- [3] USEPA, National Primary Drinking Water Standards, EPA, 816-F-03-016, 2003. Available from: <<http://www.epa.gov/safewater/consumer/pdf/mcl.pdf>>.
- [4] R. Sabry, A. Hafez, M. Khedr, A. El-Hassanin, Removal of lead by an emulsion liquid membrane, *Desalination* 212(1–3) (2007) 165–175.
- [5] H.A. Aziz, M.N. Adlan, K.S. Ariffin, Heavy metals (Cd, Pb, Zn, Ni, Cu and Cr(III)) removal from water in Malaysia: Post treatment by high quality limestone, *Bioresour. Technol.* 99 (2008) 1578–1583.
- [6] Y. Liu, J. Yan, D. Yuan, Q. Li, X. Wu, The study of lead removal from aqueous solution using an electrochemical method with a stainless steel net electrode coated with single wall carbon nanotubes, *Chem. Eng. J.* 218 (2013) 81–88.
- [7] Y. Huang, S. Li, J. Chen, X. Zhang, Y. Chen, Adsorption of Pb(II) on mesoporous activated carbons fabricated from water hyacinth using H_3PO_4 activation: Adsorption capacity, kinetic and isotherm studies, *Appl. Surf. Sci.* 293 (2014) 160–168.
- [8] M. Naushad, Z.A. ALOthman, Inamuddin, H. Javadian, Removal of Pb(II) from aqueous solution using ethylene diamine tetra acetic acid-Zr(IV) iodate composite cation exchanger: Kinetics, isotherms and thermodynamic studies, *J. Ind. Eng. Chem.* 25 (2015) 35–41.
- [9] A. Shahat, M.R. Awual, M.A. Khaleque, M.Z. Alam, M. Naushad, A.M.S. Chowdhury, Large-pore diameter nano-adsorbent and its application for rapid lead(II) detection and removal from aqueous media, *Chem. Eng. J.* 273 (2015) 286–295.
- [10] M. Naushad, Z.A. ALOthman, M.R. Awual, M.M. Alam, G.E. Eldesoky, Adsorption kinetics, isotherms, and thermodynamic studies for the adsorption of Pb^{2+} and Hg^{2+} metal ions from aqueous medium using Ti (IV) iodovanadate cation exchanger, *Ionics* 21 (2015) 2237–2245.
- [11] M. Naushad, Z.A. ALOthman, Separation of toxic Pb^{2+} metal from aqueous solution using strongly acidic cation-exchange resin: Analytical applications for the removal of metal ions from pharmaceutical formulation, *Desalin. Water Treat.* 53(8) (2015) 2158–2166.
- [12] M. Momčilović, M. Purenović, A. Bojić, A. Zarubica, M. Randelović, Removal of lead(II) ions from aqueous solutions by adsorption onto pine cone activated carbon, *Desalination* 276 (2011) 53–59.

- [13] M. Naushad, M.R. Khan, Z.A. AlOthman, I. AlSohaimi, F. Rodriguez-Reinoso, T.M. Turki, R. Ali, Removal of BrO_3^- from drinking water samples using newly developed agricultural waste-based activated carbon and its determination by ultra-performance liquid chromatography-mass spectrometry, *Environ. Sci. Pollut. Res.* 22 (2015) 15853–15865.
- [14] L. Mouni, D. Merabet, A. Bouzaza, L. Belkhir, Adsorption of Pb(II) from aqueous solutions using activated carbon developed from Apricot stone, *Desalination* 276 (2011) 148–153.
- [15] K.G. Sreejalekshmi, K.A. Krishnan, T.S. Anirudhan, Adsorption of Pb(II) and Pb(II)-citric acid on sawdust activated carbon: Kinetic and equilibrium isotherm studies, *J. Hazard. Mater.* 161 (2009) 1506–1513.
- [16] Z.-H. Huang, F. Zhang, M.-X. Wang, R. Lv, Growth of carbon nanotubes on low-cost bamboo charcoal for Pb (II) removal from aqueous solution, *Chem. Eng. J.* 184 (2012) 193–197.
- [17] M.H.M.A. Kamal, W.M.K.W.K. Azira, M. Kasmawati, Z. Haslizaidi, W.N.W.S. Saime, Sequestration of toxic Pb(II) ions by chemically treated rubber (*Hevea brasiliensis*) leaf powder, *J. Env. Sci.* 22(2) (2010) 248–256.
- [18] L. Giraldo, J.C. Moreno-Piraján, Pb^{2+} adsorption from aqueous solutions on activated carbons obtained from lignocellulosic residues, *Braz. J. Chem. Eng.* 25 (2008) 143–151.
- [19] S. Elanza, A. Lebkiri, S. Marzak, E.H. Rifi, M. Lebkiri, C. Satif, Removal of lead ions from aqueous solution by the sugarcane bagasse, *J. Mater. Environ. sci.* 5(5) (2014) 1591–1598.
- [20] V.K. Gupta, I. Ali, Removal of lead and chromium from wastewater using bagasse fly ash—A sugar industry waste, *J. Colloid Interface Sci.* 271 (2004) 321–328.
- [21] M.C. Tonucci, L.V.A. Gurgel, S.F. Aquino, Activated carbons from agricultural byproducts (pine tree and coconut shell), coal, and carbon nanotubes as adsorbents for removal of sulfamethoxazole from spiked aqueous solutions: Kinetic and thermodynamic studies, *Ind. Crops Prod.* 74 (2015) 111–121.
- [22] C. Song, S. Wu, M. Cheng, P. Tao, M. Shao, G. Gao, Adsorption studies of coconut shell carbons prepared by KOH activation for removal of lead(II) from aqueous solutions, *Sustainability* 6 (2014) 86–98.
- [23] A. Kamari, S.N.M. Yusoff, F. Abdullah, W.P. Putra, Biosorptive removal of Cu(II), Ni(II) and Pb(II) ions from aqueous solutions using coconut dregs residue: Adsorption and characterisation studies, *J. Environ. Chem. Eng.* 2 (2014) 1912–1919.
- [24] L. Largitte, J. Laminie, Modelling the lead concentration decay in the adsorption of lead onto a granular activated carbon, *J. Environ. Chem. Eng.* 3 (2015) 474–481.
- [25] V.O.S. Neto, A.G. Oliveira, R.N.P. Teixeira, M.A.A. Silva, P.T.C. Freire, D.D. Keukeleire, R.F. Nascimento, Use of coconut bagasse as alternative adsorbent for separation of copper(II) ions from aqueous solutions: Isotherms, kinetics, and thermodynamic studies, *BioResources* 6(3) (2011) 3376–3395.
- [26] S. Brunauer, L.S. Deming, W.E. Deming, E. Teller, On a theory of van der Waals adsorption of gases, *J. Am. Chem. Soc.* 62 (1940) 1723–1732.
- [27] H. Darmstadt, C. Roy, S. Kaliaguine, S. Choi, R. Ryoo, Surface Chemistry of Mesoporous Carbon Molecular Sieves. Carbon, International Carbohydrate Symposium, Lexington, KY, July 14–19, 2001.
- [28] S. Villar-Rodil, R. Denoyel, J. Rouquerol, A. Martínez-Alonso, J.M.D. Tascón, Porous texture evolution in nomex-derived activated carbon fibers, *J. Colloid Interface Sci.* 252 (2002) 169–176.
- [29] S. Yao, J. Zhang, D. Shen, R. Xiao, S. Gu, M. Zhao, J. Liang, Removal of Pb(II) from water by the activated carbon modified by nitric acid under microwave heating, *J. Colloid Interface Sci.* 463 (2016) 118–127.
- [30] M. Sekar, V. Sakthi, S. Rengaraj, Kinetics and equilibrium adsorption study of lead(II) onto activated carbon prepared from coconut shell, *J. Colloid Interface Sci.* 279 (2004) 307–313.
- [31] S.-M. Lee, C. Laldawngliana, D. Tiwari, Iron oxide nano-particles-immobilized-sand material in the treatment of Cu(II), Cd(II) and Pb(II) contaminated waste waters, *Chem. Eng. J.* 195–196 (2012) 103–111.
- [32] S.E.A. Sharaf El-Deen, F. Zhang, Synthesis of sludge@carbon nanocomposite for the recovery of As(V) from wastewater, *Proc. Environ. Sci.* 16 (2012) 378–390.
- [33] I. Langmuir, The constitution and fundamental properties of solids and liquids, *J. Am. Chem. Soc.* 38 (1916) 2221–2295.
- [34] H.M.F. Freundlich, Über die adsorption in lösungen, *Z. Phys. Chem.* 57 (1906) 385–470.
- [35] M.I. Temkin, Adsorption equilibrium and the kinetics of processes on non-homogeneous surfaces and in the interaction between adsorbed molecules, *Zh. Fiz. Khim.* 15 (1941) 296–332.
- [36] M.M. Dubinin, E.D. Zaverina, L.V. Radushkevich, Sorption and structure of active carbons. I. Adsorption of organic vapors, *Zh. Fiz. Khim.* 21 (1947) 1351–1362.
- [37] C.-V. Gherasim, G. Bourceanu, D. Timpu, Experimental and modeling studies of lead(II) sorption onto a polyvinyl-chloride inclusion membrane, *Chem. Eng. J.* 172 (2011) 817–827.
- [38] M.R. Mahmoud, G.E. Sharaf El-deen, M.A. Soliman, Surfactant-impregnated activated carbon for enhanced adsorptive removal of Ce(IV) radionuclides from aqueous solutions, *Ann. Nucl. Energy* 72 (2014) 134–144.
- [39] R.M. Seid, O. Hensel, Experimental evaluation of sorption isotherms of chili pepper: An Ethiopian variety, Mareko Fana (*Capsicum annum* L.), *Agric. Eng. Int. Cigr. J.* 14 (2012) 163–172.
- [40] M. Naushad, T. Ahamad, Z.A. AlOthman, M.A. Shar, N.S. AlHokbany, S.M. Alshehri, Synthesis, characterization and application of curcumin formaldehyde resin for the removal of Cd^{2+} from wastewater: Kinetics, isotherms and thermodynamic studies, *J. Ind. Eng. Chem.* 29 (2015) 78–86.
- [41] M.R. Awual, M.M. Hasan, A. Shahat, M. Naushad, H. Shiwaku, T. Yaita, Investigation of ligand immobilized nano-composite adsorbent for efficient cerium(III) detection and recovery, *Chem. Eng. J.* 265 (2015) 210–218.
- [42] X. Song, H. Liu, L. Cheng, Y. Qu, Surface modification of coconut-based activated carbon by liquid-phase oxidation and its effects on lead ion adsorption, *Desalination* 255 (2010) 78–83.

- [43] M.R. Mahmoud, M.A. Soliman, K.F. Allan, Adsorption behavior of samarium(III) from aqueous solutions onto PAN@SDS core-shell polymeric adsorbent, *Radiochim. Act.* 103(6) (2015) 443–456.
- [44] V.C. Srivastava, M.M. Swamy, I.D. Mall, B. Prasad, I.M. Mishra, Adsorptive removal of phenol by bagasse fly ash and activated carbon: Equilibrium, kinetics and thermodynamics, *Colloids Surf. A* 272 (2006) 89–104.
- [45] B. Subramanyam, D. Ashutosh, Adsorption isotherm modeling of phenol onto natural soils—Applicability of various isotherm models, *Int. J. Environ. Res.* 6(1) (2012) 265–276.
- [46] S. Gueu, B. Yao, K. Adouby, G. Ado, Kinetics and thermodynamics study of lead adsorption on activated carbons from coconut and seed hull of the palm tree, *Int. J. Environ. Sci. Technol.* 4(1) (2007) 11–17.
- [47] O. Olanipekun, A. Oyefusi, G.M. Neelgund, A. Oki, Adsorption of lead over graphite oxide, *Spectrochim. Acta Part A* 118 (2014) 857–860.
- [48] B. Guo, F. Deng, Y. Zhao, X. Luo, S. Luo, C. Au, Magnetic ion-imprinted and –SH functionalized polymer for selective removal of Pb(II) from aqueous samples, *Appl. Surf. Sci.* 292 (2014) 438–446.
- [49] A.K. Kushwaha, N. Gupta, M.C. Chattopadhyaya, Adsorption behavior of lead onto a new class of functionalized silica gel, *Arab. J. Chem.* (in press), doi: 10.1016/j.arabjc.2012.06.010.
- [50] S. Pitsari, E. Tsoufakis, M. Loizidou, Enhanced lead adsorption by unbleached newspaper pulp modified with citric acid, *Chem. Eng. J.* 223 (2013) 18–30.
- [51] I.M. Ahmed, A.A. Helal, N.A. El Aziz, R. Gamal, N.O. Shaker, A.A. Helal, Influence of some organic ligands on the adsorption of lead by agricultural soil, *Arab. J. Chem.* (in press), doi: 10.1016/j.arabjc.2015.03.012.
- [52] V. Venkatesham, G.M. Madhu, S.V. Satyanarayana, H.S. Preetham, Adsorption of lead on gel combustion derived nano ZnO, *Procedia Eng.* 51 (2013) 308–313.
- [53] R.P.S. Jeyakumar, V. Chandrasekaran, Adsorption of lead(II) ions by activated carbons prepared from marine green algae: Equilibrium and kinetics studies, *Int. J. Ind. Chem.* 5 (2014) 2–9, doi: 10.1186/2228-5547-5-2.
- [54] R. Leyva-Ramos, M.S. Berber-Mendoza, J. Salazar-Rabago, R.M. Guerrero-Coronado, J. Mendoza-Barron, Adsorption of lead(II) from aqueous solution onto several types of activated carbon fibers, *Adsorption* 17 (2011) 515–526.
- [55] F. Bouhamed, Z. Elouear, J. Bouzid, B. Ouddane, Batch sorption of Pb(II) ions from aqueous solutions using activated carbon prepared from date stones: Equilibrium, kinetic, and thermodynamic studies, *Desalin. Water Treat.* 52(10–12) (2014) 2261–2271.
- [56] S. Lagergren, About the theory of so-called adsorption of soluble substance, *Kungliga Svenska Vetenskaps-Akademiens Handlingar* 24 (1898) 1–39.
- [57] Y.S. Ho, Second-order kinetic model for the sorption of cadmium onto tree fern: A comparison of linear and non-linear methods, *Water Res.* 40 (2006) 119–125.
- [58] S.E.A. Sharaf El-Deen, K.F. Allan, M. Holeil, G.E.A. Sharaf El-Deen, Preparation of titanate nanoflower for sorption of ⁷⁵Se(IV) radioisotope from aqueous solution: Equilibrium, kinetic and thermodynamic studies, *Radiochim. Act.* 103(12) (2015) 843–858.
- [59] A. Murugesan, T. Vidhyadevi, S.S. Kalaivani, K.V. Thiruvengadaravi, L. Ravikumar, C.D. Anuradha, S. Sivanesan, Modelling of lead(II) ion adsorption onto poly(thiourea imine) functionalized chelating resin using response surface methodology (RSM), *J. Water Process Eng.* 3 (2014) 132–143.
- [60] S.Y. Elovich, O.G. Larinov, Theory of adsorption from solutions on non electrolytes on solid(I) equation adsorption from solutions and the analysis of its simplest form, (II) verification of the equation of adsorption isotherm from solutions, *Izv. Akad. Nauk. SSSR, Otd. Khim. Nauk.* 2 (1962) 209–216.
- [61] V.V. Grudić, Đ. Perić, N.Z. Blagojević, V.L. Vukašino-vić-Pešić, S. Brašanac, B. Mugoša, Pb(II) and Cu(II) sorption from aqueous solutions using activated red mud—Evaluation of kinetic, equilibrium, and thermodynamic models, *Pol. J. Environ. Stud.* 22 (2013) 377–385.
- [62] Z.L. Yaneva1, B.K. Koumanova, S.J. Allen, Applicability comparison of different kinetic/diffusion models for 4-nitrophenol sorption on *Rhizopus oryzae* dead biomass, *Bulg. Chem. Comm.* 45 (2013) 161–168.
- [63] J. Taparcevska, L. Markovska, B. Koumanova, V. Meshko, Diffusion models for adsorption kinetics of Zn²⁺, Cd²⁺ and Pb²⁺ onto natural zeolite, *Water Sci. Technol.* 62(5) (2010) 1136–1142.
- [64] T. Motsi, N.A. Rowson, M.J.H. Simmons, Kinetic studies of the removal of heavy metals from acid mine drainage by natural zeolite, *Int. J. Miner. Process.* 101 (2011) 42–49.
- [65] Y.S. Ho, Removal of copper ions from aqueous solution by tree fern, *Water Res.* 37 (2003) 2323–2330.
- [66] M.A. Malana, R.B. Qureshi, M.N. Ashiq, Adsorption studies of arsenic on nano aluminium doped manganese copper ferrite polymer (MA, VA, AA) composite: Kinetics and mechanism, *Chem. Eng. J.* 172 (2011) 721–727.
- [67] Y. Pang, G. Zeng, L. Tang, Y. Zhang, Y. Liu, X. Lei, Z. Li, J. Zhang, Z. Liu, Y. Xiong, Preparation and application of stability enhanced magnetic nanoparticles for rapid removal of Cr(VI), *Chem. Eng. J.* 175 (2011) 222–227.
- [68] T. Suzuki, T. Hatsushika, M. Miyake, Synthetic hydroxyapatites as inorganic cation exchangers. Part 2, *J. Chem. Soc., Faraday Trans. 1* 78(12) (1982) 3605–3611.